Available online at www.sciencedirect.com
SCIENCE DIRECT
Journal of Crystal Growth 291 (2006) 290–300
JOURNAL OF CRYSTAL GROWTH
www.elsevier.com/locate/jcrysgro

Deposition and characterization of ternary thin films within the Ti–Al–C system by DC magnetron sputtering

O. Wilhelmsson[a,*], J.-P. Palmquist[a,1], E. Lewin[a], J. Emmerlich[b], P. Eklund[b], P.O.Å. Persson[b,2], H. Högberg[b], S. Li[b,3], R. Ahuja[c], O. Eriksson[c], L. Hultman[b], U. Jansson[a]

[a]*Department of Materials Chemistry, The Ångström Laboratory, Uppsala University, P.O. Box 538, SE-751 21 Uppsala, Sweden*
[b]*Department of Physics, IFM, Thin Film Physics Division, Linköping University, SE-581 83 Linköping, Sweden*
[c]*Uppsala University, Dept. of Physics, The Ångström Laboratory, P.O. Box 530, SE-751 21 Uppsala, Sweden*

Received 3 October 2005; received in revised form 26 February 2006; accepted 1 March 2006
Communicated by G.B. McFadden

Abstract

The formation of ternary compounds within the Ti–Al–C system was studied by magnetron sputtering for thin-film deposition and first-principles calculations for phase stability. As-deposited films were characterized with X-ray diffraction (XRD) and high-resolution transmission electron microscopy (TEM). The hardness and Young's moduli of the material were studied by nanoindentation. Epitaxial and phase-pure films of $M_{n+1}AX_n$ phases Ti_3AlC_2 and Ti_2AlC as well as the perovskite phase Ti_3AlC were deposited on $Al_2O_3(00\ell)$ wafers kept at temperatures between 800 and 900 °C. The only ternary phases observed at low temperatures (300 °C) were Ti_3AlC and cubic (Ti,Al)C, the latter can be described as a metastable solid solution of Al in TiC similar to the more studied (Ti,Al)N system. The difficulties to form MAX phases at low substrate temperatures were attributed of requirement for a sufficient diffusivity to partition the elements corresponding to the relatively complex crystal structures with long *c*-axes. While MAX-phase synthesis at 800 °C is significantly lower than contemporary bulk sintering processes, a reduction of the substrate temperature towards 300 °C in the present thin-film deposition experiments resulted in stacking sequence variations and the intergrowth of (Ti,Al)C.

Keywords: A1. Solid solutions; A3. PVD; B1. Carbides; B1. MAX-phase; B1. Perovksite

1. Introduction

The Ti–Al–C system includes several ternary phases with potential in thin-film applications. For example, at least two so-called MAX phases have been identified [1,2]. The MAX phases have the general composition $M_{n+1}AX_n$, ($n = 1$–3) where M is a transition metal, A is an element from group 13–14 and X is either carbon or nitrogen. These compounds were originally synthesized in the 1960s [2,3], but they have been given an increased attention since 1995 when Barsoum et al. [4] discovered that they exhibit unique physical and chemical properties. The structure of the MAX phases can be described as nanolaminates of MX slabs separated by square-planar layers of the A-element. The M–A bonds are weaker than the M–X bonds within the slabs. This gives rise to a strongly anisotropic and nanolaminated structure with unusual mechanical properties. Theoretical and experimental studies on the MAX phases show that they are, e.g., machinable, resistant to thermal shock, and thermally and electrically conductive [5–11]. This combination of properties makes these compounds interesting in thin-film applications such as electrical contacts and low friction materials, as well as in bulk applications, e.g., high-temperature materials [12,13].

In the Ti–Al–C system, there is a single phase area of the MAX phase Ti_2AlC (denoted H in the phase diagram

*Corresponding author. Tel.: +46 18 4713769; fax: +46 18 513548.
E-mail address: Ola.Wilhelmsson@mkem.uu.se (O. Wilhelmsson).
[1]Present address: Kanthal AB, P.O. Box 502, SE-734 27 Hallstahammar, Sweden.
[2]Present address: FEI Company, Achtseweg Noord 5, Building AAE, 5651 GG Eindhoven/Acht, The Netherlands.
[3]Present address:Department of Physics, Virginia Commonwealth University, Richmond, VA 23284, USA.

0022-0248/$ - see front matter © 2006 Elsevier B.V. All rights reserved.
doi:10.1016/j.jcrysgro.2006.03.008

presented in Fig. 1) [14]. The unit cell of this phase can be described as slabs of TiC where each slab consists of two Ti planes separated by planar layers of Al. However, Pietzka et al. [15] have synthesized a second MAX phase Ti_3AlC_2 where the TiC slabs contain 3 Ti-planes. Although Ti_3AlC_2 is not found in the reported phase diagram, it can be synthesized indicating a small homogeneity range and a lower stability than Ti_2AlC. However, today the reported phase diagram of the Ti–Al–C system may be necessary to redraw to also take the Ti_3AlC_2 phase into consideration. The properties of the MAX phases Ti_3AlC_2 and Ti_2AlC have been studied for bulk samples.

The Ti–Al–C system also includes a ternary carbide with the composition Ti_3AlC (denoted P in Fig. 1). This phase has a perovskite structure similar to oxide perovskites. In the crystal structure Ti and Al form an fcc-like structure with C in the body-centered octahedral hole [16,17]. Ti_3AlC is frequently formed as precipitations in bulk samples [18], but the physical properties of this compound need to be further investigated. It should be noted, however, that this type of perovskite carbide may exhibit superconductivity [19]. The combination of superconductivity and excellent mechanical properties (e.g., high strength) makes these compounds potential candidates for superconducting applications [20].

As can be seen in Fig. 1, most of the binary phases, e.g., TiC in the Ti–Al–C system show a very limited solid solubility of the third component at equilibrium. However, thin-film processes such a magnetron sputtering can be carried out at reduced temperatures where the diffusion rates of the elements are low. This makes it possible to deposit ternary solid solutions of binary phases where the solubility of the third element widely exceeds the maximum equilibrium solubility. These films are metastable, but may exhibit improved physical and chemical properties compared to the thermodynamically stable phases and therefore can be highly interesting for many thin-film applications. For example, metastable (Ti,Al)N films are widely used as wear-resistant coatings containing as much as 60 at% Al on the metal side [21]. The improved properties are partly given to the formation of a protecting aluminum oxide layer at higher temperatures [22]. Furthermore, Hörling et al. [23] has demonstrated that metastable ternary Ti–Al–N films deposited at low temperatures can age harden into TiN and the metastable NaCl-structure of AlN before eventual precipitation of wurtzite-AlN. This process yields a spontaneous hardening of the film due to coherency strain between the TiN–AlN domains [23]. Due to the structural similarities, we suggest that metastable solid solutions can also be formed in the Ti–Al–C thin-film system and that a careful annealing process can control the properties of these films.

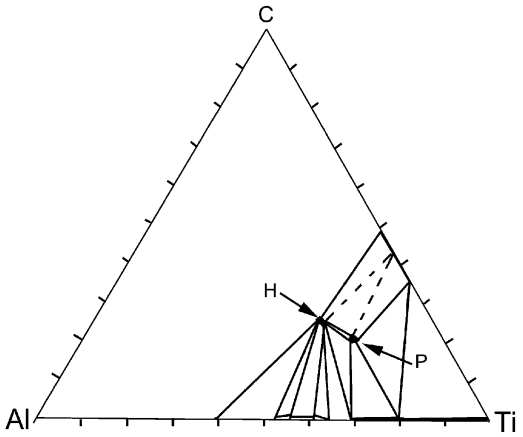

Fig. 1. Isothermal section of the Ti–Al–C system at 1000 °C (from Ref. [14]).

Our initial study on thin-film deposition in the ternary Ti–Al–C system showed the feasibility of using DC magnetron sputtering to make MAX phases from this system [24]. The objective with this study is to carry out a more detailed investigation of ternary films in the Ti–Al–C system including characterization with electron microscopy and nanoindentation measurements. The experimental study has also been combined with ab initio calculations of the MAX phases. In particular, the phase stability in the $Ti_{n+1}AlC_n$ system and the possibility to deposit other MAX-phases than Ti_3AlC_2 and Ti_2AlC was investigated.

2. Experimental procedure

Ti–Al–C films were deposited in ultra high-vacuum (base pressure $<10^{-9}$ Torr) employing DC magnetron sputtering from elemental 2″ targets of Ti, Al and C with a purity of 99.995%, 99.999%, and 99.99%, respectively. The fluxes were controlled by the magnetron current. The Ti current was kept constant at 220 mA and the C and Al currents were varied between 130–185 mA and 30–50 mA, respectively. All films were deposited on α-$Al_2O_3(0\,0\,\ell)$ substrates. Prior to deposition the substrates were ultrasonically degreased for 5 min periods in trichloroethylene, acetone and iso-propanol and pre-heated, in the deposition chamber, at 500 °C for 1 h. To promote the growth of both the MAX phases and the perovskite a 200 Å thick seed layer of $TiC_{0.7}(\ell\,\ell\,\ell)$ was initially deposited on the substrates. Subsequently, the Al target was started to initiate the growth of the MAX phase and the perovskite, respectively. The deposition rate was about 25 Å/min and most of the films were deposited for an hour to a thickness of ~1500 Å.

The composition was investigated ex situ by X-ray photoelectron spectroscopy (XPS) using a PHI Quantum 2000 instrument with monochromatizied Al-Kα radiation. The quantitative analysis was carried out using a Ti–Al–C standard sample for calibration of the sensitivity factors.

The phase composition and epitaxial relations were studied by X-ray diffraction (XRD) using a Simens D5000 diffractometer for θ–2θ and Gracing Incident (GI) scans and a Philips X'pert instrument for reciprocal space maps (RSM), both using Cu-Kα radiation.

The microstructure of cross-sectional samples was studied with high-resolution transmission electron microscopy

(HR-TEM) using a FEI Tecnai F30 ST equipped with Energy dispersive X-ray (EDX).

Nanoindentation experiments were performed at room temperature employing a Triboscope® (Hysitron Inc.) and a Nanoindenter XP on 6000 Å thick films. The Oliver and Pharr method was employed to calculate hardness and Young's moduli values [25].

3. Calculations

Within the MAX-phase family, several theoretical investigations have been carried out to understand, e.g., the influence of different transition metals on the bulk modulus [11,26], the stability of the ternary compounds compared to their binary equilibrium phases [27], electronic properties [28], and solid solutions of iso-structures [29]. In this study, we have used the Vienna ab initio simulation package (VASP) and projector augmented wave (PAW) potentials to calculate cohesive energies and bulk moduli of MAX phases in the Ti–Al–C system [30]. A cutoff energy of 500 eV for the plane-wave basis was used. The Brillouin zone integration was carried out using a $9\times9\times9$ k-point grid. The total energies were converged to below 0.001 eV as regards the number of k-points. The tetrahedron method with Blöchl corrections was applied for both geometry relaxation and total energy calculations. The geometry optimization was considered to be converged when the total force on the atoms was less than 1×10^{-4} eV/Å. The equilibrium volume and bulk moduli for the different MAX-phases were calculated by fitting the calculated volume and energy values to Birch–Murnaghan's equation of states [31].

Table 1 lists the calculated cell parameters, bulk moduli and cohesive energies for TiC, Ti_2AlC, Ti_3AlC_2 and the hypothetical MAX phase Ti_4AlC_3. The different MAX phases can be described based on the number of Al-layers per Ti-layer. With this description, Ti_3AlC_2 and Ti_2AlC have 0.33 and 0.50 Al-layers per Ti-layer, respectively. This also means that the relative strength of the Ti–C and Ti–Al bonds will be important for the properties of the MAX phases. Since the Ti–Al bond is considerably weaker than the Ti–C bond, an increase in the number of inserted Al-layers per Ti-layer should, in principle, give a less stiff material. This was also observed in the calculations, which gave a weakly non-linear relationship between the bulk moduli and number of inserted Al-layers (see Fig. 2). A similar relationship is observed for the Ti–Si–C system. The bulk moduli for the MAX phases within the Ti–Si–C system is, however, larger than in the Ti–Al–C system since the bond strength between Ti–Al is weaker than Ti–Si [32].

In Table 1 it can be seen that the cohesive energy for the MAX phases approaches the value for TiC as the number of Al-layers decreases, i.e. the MAX phase becomes more "TiC-like". Fig. 3 shows the cohesive energy difference between the Ti–Al–C MAX phases and TiC calculated and presented in Table 1. The same energy difference, calculated by Li et al. [27] for the Ti–Si–C system, is also plotted in Fig. 3. The slope of the curve is an indication of the energy cost of the insertion of A-layers in between the TiC-slabs. As can be seen in the figure, the Ti–Al–C system initially has a steeper slope than the Ti–Si–C system. Once more, this is due to the fact that the Ti–Al bond is weaker than the Ti–Si bond and that the energy "cost" to insert an Al layer therefore is higher than for a corresponding Si-layer. Another interesting observation is that the curve for the Ti–Si–C system is more or less linear. This suggests that

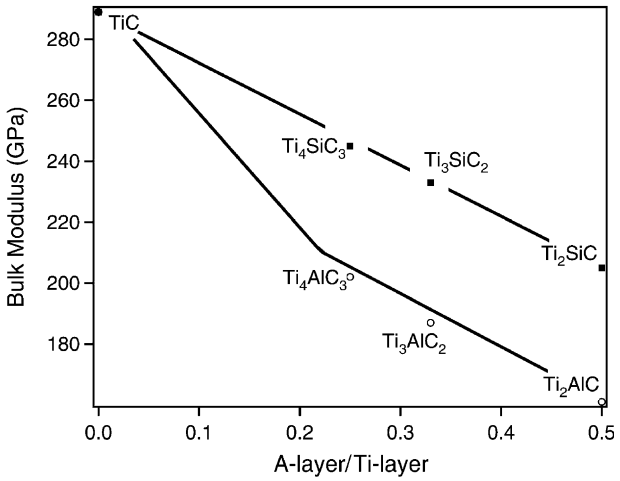

Fig. 2. Bulk moduli from ab initio calculations for the Ti–A–C (A = Si or Al) system as a function of inserted A-layers. The curves are guide for the eye only.

Table 1
Calculated bulk moduli and cell parameters for $Ti_{n+1}AlC_n$ phases, and cohesive energy (Ecoh) and difference in cohesive energy between $Ti_{n+1}AlC_n$ phases and TiC

Phase	Al-layer/Ti-layer	Bulk modulus (GPa)	E_{coh} (eV/atom)	E_{MAX}-E_{TiC} (eV/atom)	Cell parameters			
					Calculated		Measured	
					a-axis (Å)	c-axis (Å)	a-axis (Å)	c-axis (Å)
TiC	0	270	−9.2792				4.30	
Ti_4AlC_3	0.25	202	−8.5572	0.722	3.06	23.60		
Ti_3AlC_2	0.33	187	−8.3187	0.960	3.06	18.67	3.06	18.59
Ti_2AlC	0.5	161	−7.7935	1.485	3.04	13.61	3.04	13.59

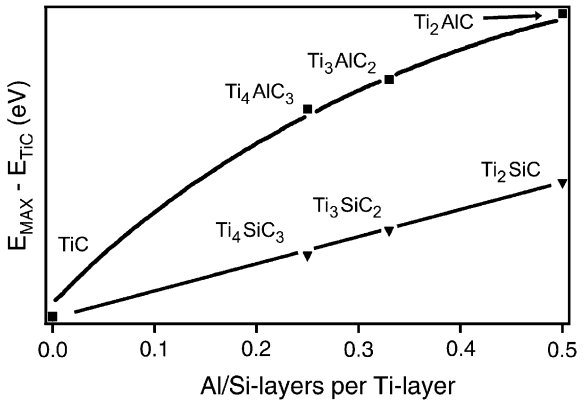

Fig. 3. Cohesive energy from ab initio calculations for the Ti–A–C (A = Si or Al) system as a function of inserted A-layers. The curves are guide for the eye only.

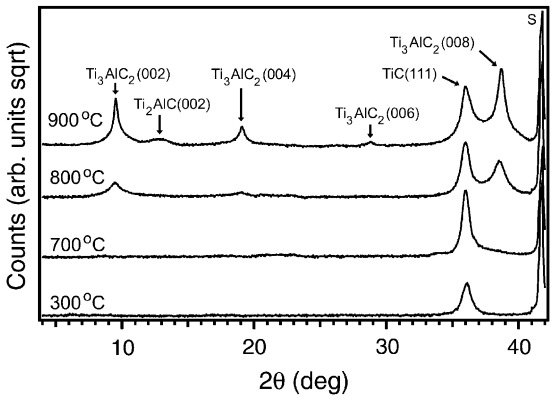

Fig. 4. θ–2θ diffractograms from Ti–Al–C films with a composition of 50 at% Ti, 16 at% Al and 34 at% C deposited on $Al_2O_3(0\,0\,\ell)$ wafers as a function of substrate temperature between 300 and 900 °C. Substrate peak is denoted "S".

the average energy required to insert a Si-layer is independent on the number of layers. One interpretation of this behavior is that random stacking sequences could be expected. This has also been observed experimentally in magnetron sputtered Ti–Si–C films. In contrast, the corresponding curve for the Ti–Al–C system in Fig. 3 exhibits a weakly non-linear behavior that suggests that it is more favorable with a higher density of inserted Al-layers (i.e. Ti_2AlC is more stable than Ti_3AlC_2). It should be noted that the true stability of the MAX phases are also dependent on the sign of ΔG in an assumed reaction compared to competing phases.

4. Experimental results and discussion

4.1. General observations

Ti–Al–C thin films were deposited in the temperature range 300–900 °C. The MAX phases Ti_3AlC_2 and Ti_2AlC were only deposited at temperatures above 800 °C. This can be seen in Fig. 4, which shows θ–2θ diffractograms from films with a total composition of 50 at% Ti, 16 at% Al and 34 at% C determined by XPS measurements (i.e., corresponding to a total composition of Ti_3AlC_2). At 900 °C only peaks of the $\{0\,0\,\ell\}$ type from the MAX phase Ti_3AlC_2, the TiC($\ell\,\ell\,\ell$) seed layer and a weak peak from $Ti_2AlC(0\,0\,2)$ can be observed. As the deposition temperature was reduced the MAX phase peak intensities decrease and vanished completely below 800 °C. Instead the intensity of the TiC($\ell\,\ell\,\ell$) peak increases. At 300 °C the intensity of the TiC peaks starts to decrease and a small shift towards higher 2θ values was observed. As will be discussed in Section 4.4 this is consistent with a formation of cubic (Ti,Al)C film (i.e., a solid solution of Al in the Ti-sites in TiC). These results are in general agreement with previous studies in the Ti–Ge–C and Ti–Si–C systems, which also clearly show that an elevated substrate temperature is required for MAX-phase formation [33,34]. By tuning the composition a third ternary phase, the Ti_3AlC perovskite, was also deposited. This phase was grown between 300 and 800 °C.

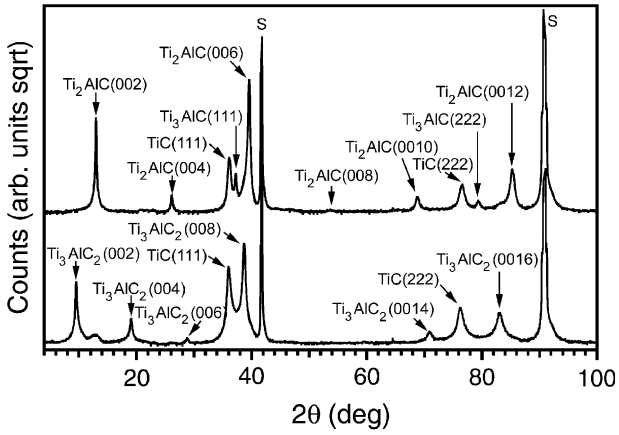

Fig. 5. θ–2θ diffractograms from 1500 Å thick epitaxial (upper curve) $Ti_2AlC(0\,0\,\ell)$ and (lower curve) $Ti_3AlC_2(0\,0\,\ell)$ films, respectively, deposited on $Al_2O_3(0\,0\,\ell)$ wafers at a substrate temperature of 900 °C. Substrate peak is denoted "S".

XPS-depth profiling of films deposited at elevated temperatures showed no indication of a composition gradient and that the bulk of the films, within the detection limit for XPS, was free from oxygen and other contaminants. Films deposited at 300 °C showed a minor content of oxygen due to a low desorption rate of oxygen during the deposition. Finally, in the X-ray analysis of the films deposited at high temperatures an indication of substrate-seed layer solid-state reaction was observed. This will be further discussed in Section 4.5.

4.2. Deposition of MAX-phase films

Fig. 5 shows θ–2θ X-ray diffractograms of 1500 Å thick Ti_2AlC and Ti_3AlC_2 films, respectively, deposited on $Al_2O_3(0\,0\,\ell)$ substrates at a temperature of 900 °C. As can be seen in Fig. 5 there are mainly peaks of the $\{0\,0\,\ell\}$ type

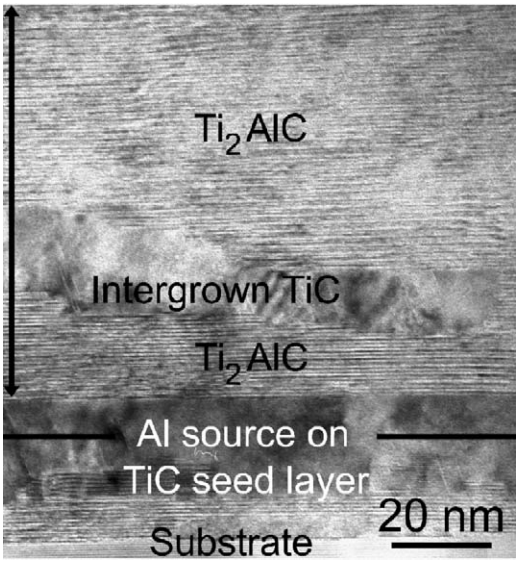

Fig. 6. Cross-sectional TEM image of an epitaxially-grown $Ti_2AlC(0\,0\,\ell)$ film. In the figure the substrate, the TiC seed layer, a TiC inclusion and the delayed nucleation of Ti_2AlC MAX-phase can be seen. The contrast arises from the characteristic structure of the MAX phase.

from the MAX phases together with $TiC(\ell\,\ell\,\ell)$ and α-$Al_2O_3(0\,0\,\ell)$. In the diffractogram from the Ti_2AlC film there is also a minor peak from $Ti_3AlC(\ell\,\ell\,\ell)$. In the diffractogram from the Ti_3AlC_2 film there is also a small contribution from Ti_2AlC. Consequently, since the weak intensity of the extra peaks we conclude that single-phase material of the MAX phases Ti_2AlC and Ti_3AlC_2 can be deposited at this temperature.

The observation of only peaks of the $\{0\,0\,\ell\}$ type from the MAX phases indicates a highly textured or epitaxial growth. It was confirmed by pole figures of α-$Al_2O_3(1\,0\,1\,0)$, $Ti_{n+1}AlC_n(1\,0\,1\,0)$ and $TiC(1\,5\,3)$ that the growth indeed was epitaxial with α-$Al_2O_3(0\,0\,\ell)$//$TiC(\ell\,\ell\,\ell)$//$Ti_{n+1}AlC_n(0\,0\,\ell)$ and an in-plane orientation of $Al_2O_3[2\,1\,0]$//$TiC[1\,\bar{1}\,0]$//$Ti_{n+1}AlC_n[2\,1\,0]$ and $Al_2O_3[2\,1\,0]$//$TiC[\bar{1}\,1\,0]$//$Ti_{n+1}AlC_n[2\,1\,0]$. This in-plane orientation corresponds to a 30° rotation of the hexagonal phase relative to the cubic phase. The rotation can be expected since the [2 1 1 0] direction is a close packed direction in the hexagonal basal plane. By RSM the cell parameters and the presence of possible stress were studied. By mapping of three asymmetrical peaks of the Ti_3AlC_2 and Ti_2AlC films, the cell parameters were determined to $a = 3.07$ Å and $c = 18.59$ Å, and $a = 3.04$ Å and $c = 13.59$ Å, respectively. This is in agreement with our theoretical calculations summarized in Table 1 and with previous values on bulk samples published in the literature [5]. From RSM it was also concluded that the MAX-phase layers are relaxed towards the TiC seed layer with respect to coherency strain.

Fig. 6 shows an overview cross-sectional TEM micrograph of an epitaxial Ti_2AlC film with the beam parallel to the [1 1 0] direction. In the upper part of the figure bright bands separated by thin black lines can be seen. This contrast arises due to the characteristic structure of the MAX phase with TiC slabs interleaved by square planar A-layers. High-resolution micrographs show the characteristic stacking sequence for Ti_2AlC with two Ti(C) layers separated with a single Al-layer. The films contain regions of a cubic phase intergrown in the MAX phase layer. EDX analysis in situ the TEM of these cubic regions show that they consist of (Ti,Al)C, i.e. TiC with a solid solution of Al at Ti sites. The presence of these regions suggests that the MAX phase growth is sensitive to the segregation of Al and correct partitioning of elements at the growth surface or in the topmost atomic layers. The metastable cubic solid solution may form in competition by virtue of its related crystal structure to the MAX phase simply by continuing growth of a Ti(C) layer during the deposition process.

Another observation in Fig. 6 is that the nucleation of Ti_2AlC on the TiC seed layer is delayed. When the Al target is switched on (marked with a line in Fig. 6) a cubic (Ti,Al)C layer is formed. The nucleation of the Ti_2AlC is delayed for another 50–100 Å. Indeed TEM EDX of the incubation region shows from the point where the Al target is switched on, an increasing concentration of Al in the cubic (Ti,Al)C layer. After about 50 Å the concentration of Al has reached a level that corresponds to Ti_2AlC and nucleation of this phase can start. The formation of the (Ti,Al)C incubation layer is thus of similar origin as the (Ti,Al)C intergrown layer described above. In both cases the XTEM images indicate that the MAX phase layer nucleates on a (Ti,Al)C(1 1 1) surface feature by the spreading surface coverage of Al. Similar nucleation and growth behavior was observed by Emmerlich et al. [33,34] for growth of $(0\,0\,\ell)$-oriented epitaxial Ti–Si–C MAX-phase films.

Fig. 7 shows a high-resolution cross-sectional TEM micrograph of a Ti_3AlC_2 film deposited at 900 °C. The typical stacking sequence for the Ti_3AlC_2 phase with three

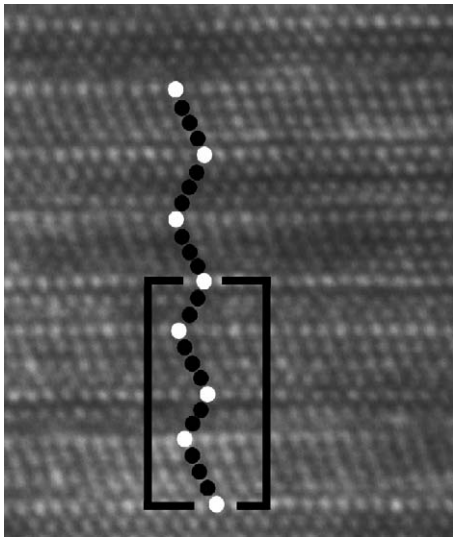

Fig. 7. High-resolution cross-sectional TEM of an epitaxially-grown $Ti_3AlC_2(0\,0\,\ell)$ film. Within the square an occasionally $Ti_5Al_2C_3$ stacking sequence can be seen. (Black circle = Ti and white circle = Al atom).

TiC-slabs interleaved with a square-planar layer of Al can be observed. However, occasionally other stacking sequences corresponding to $Ti_5Al_2C_3$ can be observed (see Fig. 7). This phase can be considered as an intergrown structure. In bulk samples Lin et al. [35] has observed intergrowth of Ti_2AlC and Ti_3AlC_2. The unit cell of $Ti_5Al_2C_3$ can be described as half a unit cell of Ti_2AlC combined with a half unit cell of Ti_3AlC_2. Thin films with this structure can be deposited in the Ti–Si–C and Ti–Ge–C systems and observed by X-ray diffraction [33,34]. In our study, however, this type of intergrowth structures is only rarely observed as local deviations in stacking sequence. In fact, growth experiments with varied compositions did not yield more intergrowth structures, but instead an equilibrium between the respective MAX and (Ti,Al)C phases. According to our calculations the cohesive energy of the MAX-phases is dependent on number of Al-layers/Ti-layers in the Ti–Al–C system. Therefore, it is less favorable to form random stacking sequences in the Ti–Al–C system than in, e.g., the Ti–Si–C system and phases as $Ti_5Al_2C_3$ is only occasionally observed (see Section 3).

Figs. 8a and b show the hardness and Young's modulus determined by nanoindentation for Ti_3AlC_2 and Ti_2AlC thin films, respectively. Allegedly substrate-independent hardness and modulus values of 20 ± 1 and 260 ± 10 GPa, respectively, were measured for both films. As the indentation load was increased to yield maximum indentation depths of 30% of the film thickness, the hardness value decreased to below 14 GPa for Ti_3AlC_2 and 15 GPa for the Ti_2AlC film. The same trend was seen for the Young's modulus, which for deeper intents was measured to

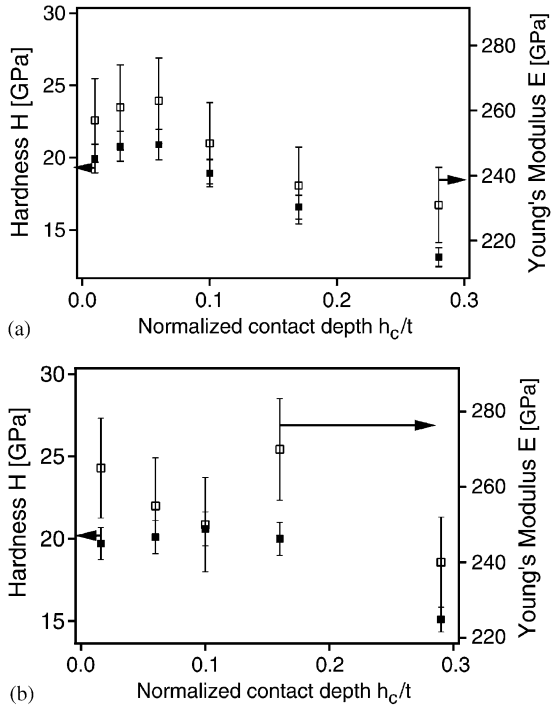

Fig. 8. Hardness and Young's modulus vs. normalized contact depth for 6000 Å thick (a) $Ti_3AlC_2(0\,0\,\ell)$ and (b) $Ti_2AlC(0\,0\,\ell)$ films.

~240 GPa for the Ti_3AlC_2 and Ti_2AlC film, respectively. A similar behavior in the mechanical properties has also been observed for other MAX-phase system, employing nanoindentation measurement on thin films and Vickers measurement on bulk samples [36–38]. This phenomenon, i.e. a decrease in hardness with increasing load, is known as indentation size effect (ISE) and is attributed to the material under study. It arises due to, e.g., influence from the native oxide [39] and critical load to initiate plastic deformation, i.e. by kink band formation in the MAX phase [40]. It should also be noted that the Al_2O_3 substrates used are both harder and stiffer than the MAX-phase layers such that the analysis made should be reliable over the range of loads studied. Therefore, a hardness value of ~15 GPa and a Young's modulus of ~240 GPa can be considered as closer to the intrinsic values of these MAX phases. It is notable that the hardness to Young's modulus ratios obtained is more comparable to the ductile metals than the ceramics.

A hardness of ~15 GPa is considerably higher than the Vickers hardness of 2.7 GPa measured by Wang et al. [38] on polycrystalline bulk samples of Ti_3AlC_2. However, these measurements were carried out on non-phase pure samples with a random crystal grain orientation, and the hardness of these compounds is expected to be quite anisotropic. Early studies on small single crystals of Ti_3SiC_2 prepared by CVD, reported Knoop hardness values normal and parallel to the basal planes of 12–15 and 3–4 GPa, respectively [41]. Our measurements on Ti_3AlC_2 films normal to the planes are in good relative agreement with these results. Furthermore, Molina et al. [42] has reported a hardness value of 15 GPa measured by nanoindentation normal to the basal planes of the MAX-phase thin films of Ti_3SiC_2, which also is in agreement with our measurement. The reported Vickers hardness of polycrystalline bulk samples of Ti_3SiC_2 range between 4 and 7 GPa depending on the indent load [43]. As for the Ti–Al–C system the hardness values between bulk and thin film samples differ due to the anisotropic structure.

The calculated bulk moduli in Fig. 2 suggest that Ti_2AlC should be less stiff than Ti_3AlC_2, due to the larger density of inserted Al-layers. Our experimentally measured values of Young's moduli, however, show a similar value for Ti_2AlC and Ti_3AlC_2. This can be explained by the fact that the calculated bulk moduli are only based on bond strengths within the structure. The experimentally determined Young's moduli on the other hand are also influenced by the characteristic deformation behavior such as delamination and kink formation in the MAX phases [40]. Also, as seen in Fig. 6, structural inhomogeneties (i.e. (Ti,Al)C inclusion) give rise to a deviation from the theoretical value.

4.3. Deposition of epitaxial Ti_3AlC

Ternary carbides with the general composition M_3AC, where M and A represent two metals, are known in many

systems including Ti–Al–C. These phases have a perovskite structure which can be described as an ordered fcc arrangement of Ti and Al with C in the body-centered octahedral sites [44]. In our study, thin films of epitaxial Ti_3AlC were deposited at 800 and 300 °C. Fig. 9 shows an example of a θ–2θ diffractogram of a 1500 Å thick perovskite Ti_3AlC film deposited on $TiC(\ell\,\ell\,\ell)//Al_2O_3(0\,0\,\ell)$ at 800 °C. In the diffractogram there are two peaks from $Ti_3AlC(1\,1\,1)$ and $Ti_3AlC(2\,2\,2)$, together with peaks from the seed layer (TiC(1 1 1) and TiC(2 2 2)), the substrate and a weak signal from $Ti_2AlC(0\,0\,2)$. Given the fact that the Ti_2AlC phase only exists as small inclusions formed by a solid-state reaction between the TiC seed layer and substrate the film can be considered as a single-phase Ti_3AlC layer. The observation of only $\{\ell\,\ell\,\ell\}$ type peaks suggests a highly textured or epitaxial growth. By X-ray pole figures it was confirmed that the growth was epitaxial with domains rotated by 180°, i.e. a stacking sequence of ABC and BCA, both in seed layer and in the perovskite. The growth was determined to be "cube-on-cube", i.e. $Ti_3AlC(\ell\,\ell\,\ell)//TiC(\ell\,\ell\,\ell)$ with the in-plane directions $Ti_3AlC[1\,1\,0]//TiC[1\,1\,0]$ and $Ti_3AlC[1\,1\,0]/TiC[\bar{1}\,\bar{1}\,0]$. This is expected since TiC and Ti_3AlC have comparable cell parameters, which in the $[\ell\,\ell\,\ell]$ direction results in a misfit of −4.2%. Consequently there are excellent conditions for epitaxial growth of this phase on a TiC seed layer. Furthermore, from RSM it was concluded that the film was completely relaxed, with a cubic cell with $a = 4.17$ Å. This value is in agreement with the literature data on the cell parameter for Ti_3AlC [16]. Furthermore, from the RSM no indication of distortions in the cubic symmetry was observed. In contrast to the MAX-phase growth, Ti_3AlC was also possible to deposit at temperatures below 800 °C. In fact, it was possible to deposit single phase and epitaxial films of Ti_3AlC at as low substrate temperatures as 300 °C.

The epitaxial growth was also confirmed by cross-sectional TEM. Micrographs revealed a dense and columnar growth of the perovskite. The columnar growth

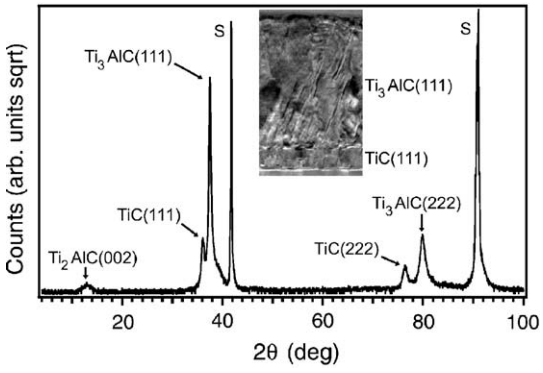

Fig. 9. θ–2θ diffractogram of a 1500 Å thick epitaxial perovskite $Ti_3AlC(\ell\,\ell\,\ell)$ film with a "cube-on-cube" growth on the seed layer of $TiC(\ell\,\ell\,\ell)$. Substrate peak is denoted "S". The inset shows a cross-sectional TEM with the TiC seed-layer (bottom) followed by the Ti_3AlC film. Columnar grains can be observed.

is not in contradiction to the observed epitaxial growth behavior since each column exhibits an epitaxial relationship to the TiC/Al_2O_3 substrate (see inset in Fig. 9).

The hardness and Young's modulus of $Ti_3AlC(\ell\,\ell\,\ell)$ were determined to be 11 and 240 GPa, respectively. These values are in the same range as for the MAX phases, but considerably lower than for pure TiC, which typically exhibit a hardness of ~30 GPa and a Young modulus of ~380 GPa [44]. There are no reports in the literature on the mechanical properties of the perovskite, but the results can be discussed based on the large structural similarities between Ti_3AlC and TiC. The perovskite can be described as solid solution of Al in a sub-stoichiometric TiC and be written as $(Ti_{0.75}Al_{0.25})C_{0.25}$. This means that the perovskite can be considered as a TiC phase where $\frac{3}{4}$ of the octahedral sites are vacant (only $\frac{1}{4}$ occupied by carbon) and $\frac{1}{4}$ of the Ti-atoms have been substituted with Al. It is well known that the hardness and stiffness of TiC is strongly reduced with an increased amount of carbon vacancies [45]. The high vacancy content in the perovskite relative to a stoichiometric TiC can then explain the lower hardness and Young's modulus of the former. Also, theoretical calculations on the Ti_3AlC phase have shown that the addition of Al reduces the directionality of the bonds and gives a higher amount of weaker Al–C bonds compared to pure TiC [17].

4.4. Deposition of cubic (Ti,Al)C films

At temperatures below 800 °C no MAX phase growth was observed. An analysis of these low-temperature films revealed that they consist of a solid solution of Al in sub-stoichiometric cubic TiC. As will be shown below, the process starts with an epitaxial growth of (Ti,Al)C films on the α-$Al_2O_3(0\,0\,\ell)$ substrate. After ~200 Å the epitaxy is lost and a polycrystalline carbide film is formed. θ–2θ diffractograms from these films only show $TiC(\ell\,\ell\,\ell)$ peaks originating from the epitaxial part of the film. This is due to the fact that the θ–2θ mode only shows peaks from planes parallel to the substrate surface that gives very high intensity. In contrast, GI X-ray diffraction measurements reveal a polycrystalline growth closer to the surface. This can be seen in Fig. 10, which shows two GI-scans from polycrystalline $(Ti_{0.75}Al_{0.25})C_{0.5}$ (Fig. 10a) and $(Ti_{0.67}Al_{0.33})C_{0.33}$ (Fig. 10b) films deposited directly on the α-$Al_2O_3(0\,0\,\ell)$ substrate at 300 °C. The inset in Fig. 10 shows the 111 peak from the θ–2θ scans and gives mainly information from the epitaxial part closer to the substrate. As can be seen, the addition of Al shifts the peaks to higher 2θ values, which is due to a reduction in size of the unit cell. From the peak position in the θ–2θ scan, the cell parameter of the epitaxial part of the $(Ti_{0.75}Al_{0.25})C_{0.5}$ and $(Ti_{0.67}Al_{0.33})C_{0.33}$ films can be determined to be 4.29 and 4.22 Å, respectively. Since the cell parameter of pure TiC depends on the stoichiometry these values should be compared with pure TiC with a similar C/Ti ratio (i.e. 0.50 and 0.33). Guemmaz et al. has reported on the cell

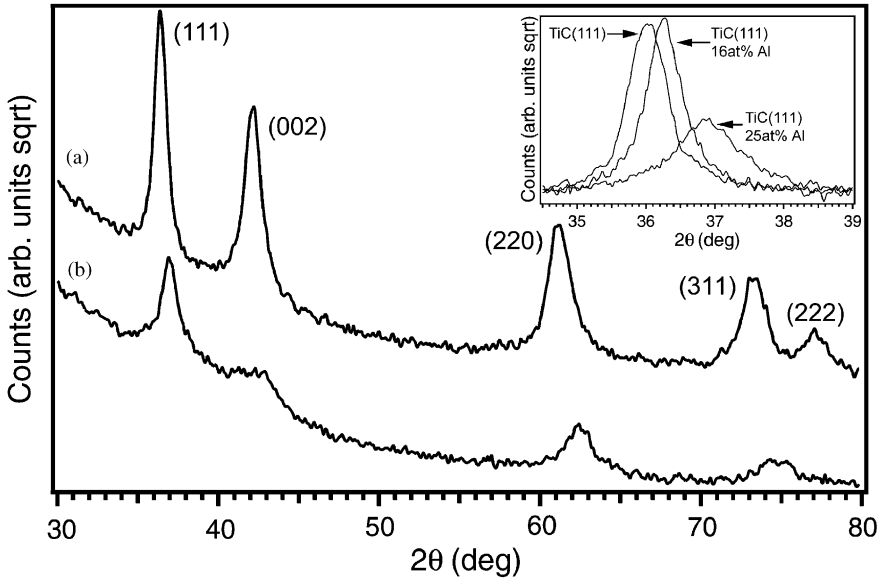

Fig. 10. GI-scans from polycrystalline (a) $(Ti_{0.75}Al_{0.25})C_{0.5}$ and (b) $(Ti_{0.67}Al_{0.33})C_{0.33}$ films deposited without a TiC seed layer at 300 °C on $Al_2O_3(0\,0\,\ell)$ substrates. The inset shows the peak shift for the corresponding θ–2θ scan of the 111 peak.

parameters of $TiC_{0.50}$ and $TiC_{0.33}$ to be 4.30 and 4.29 Å, respectively [46], i.e. significantly less than for stoichiometric TiC of 4.32 Å [47]. Our cell parameters are lower than the reported values since the solid solution of the smaller Al atom into the sub-stoichiometric TiC-lattice further reduces the size of the unit cell. The GI-scans in Fig. 10 also shows that the intensity of the peaks from the film with the lower Al concentration is higher and exhibit smaller full widths at half maximum. This indicates larger and more well-ordered crystallites. By applying Scherrer's formula to the 111 peak, the size of the crystallites were estimated to 240 and 180 Å for the $(Ti_{0.75}Al_{0.25})C_{0.5}$ and $(Ti_{0.67}Al_{0.33})C_{0.33}$ films, respectively.

Figs. 11a–c show XPS spectra of C(1 s), Ti(2p) and Al(2p) from Ar-sputter cleaned surfaces of $(Ti_{0.75}Al_{0.25})C_{0.5}$, Ti_3AlC (i.e. $(Ti_{0.75}Al_{0.25})C_{0.25}$) (see Section 4.3) and Ti_2AlC ($(Ti_{0.67}Al_{0.33})C_{0.33}$) MAX-phase films, and for comparison a phase pure $TiC_{0.67}$ film. The C(1 s) spectrum shows a peak at ~281.8 eV for all the films, which originates from carbon in the carbidic state, i.e. metal–carbon bonds. Considering that, in all films, C has an octahedral coordination of Ti a similar C(1s) position in all spectra is consistent. A small shift, however, towards higher binding energies can be seen for the Al-containing films. This shift is induced by Al–C interactions and the position can be compared with the C(1s) peak in Al_4C_3 at 282.2 eV [48]. As can be seen in Fig. 11a, there is no signal at 284 eV, which in such case often originates from amorphous matrix of non-carbide carbon. The Ti(2p) signal (see Fig. 11b) is positioned at ~454.5 eV for all films and clearly indicate a Ti–C interaction. As seen in Fig. 11c, the peak of Al(2p) is shifted towards higher binding energies and broadened with an increasing C content, i.e. going from $(Ti_{0.75}Al_{0.25})C_{0.20}$ to $(Ti_{0.75}Al_{0.25})C_{0.5}$. An increase in binding energy is explained by an increasing amount of Al–C interaction. For the $(Ti_{0.75}Al_{0.25})C_{0.50}$ and the $(Ti_{0.75}Al_{0.25})C_{0.25}$ film, Al(2p) is positioned at 73.2 and 72.4 eV, respectively. In Al_4C_3 the peak is positioned at 73.4 eV [48]. The shift is consistent with an increase in Al–C bond character in the compound. Compared to the structurally related (Ti,Al)N a similar shift is seen for the Al(2p) peak. However, that shift is larger since N is more electronegative than C and therefore more strongly attracts electrons from Al [49]. The Al(2p) peak of $(Ti_{0.67}Al_{0.33})C_{0.33}$, i.e. the Ti_2AlC MAX-phase, is positioned at 72.37 eV and with the smallest full-width at half-maximum. The binding energy of Al(2p) of Ti_2AlC and Ti_3AlC is similar although different crystal structures. This can be explained by the layer-like Al-planes in Ti_3AlC. Compared to the Al-slabs in the MAX-phase (Ti_2AlC) these layers constitutes not only of Al but are interrupted by Ti-atoms.

Fig. 12 shows a cross-sectional TEM micrograph for a film with the composition $(Ti_{0.75}Al_{0.25})C_{0.5}$. As was observed in the GI measurement and θ–2θ scan (see Fig. 10), the initial growth is epitaxial (bottom inset), which after ~200 Å changed to a polycrystalline growth behavior. The average crystallite size was estimated to be ~200 Å, which is in agreement with the values calculated by using Scherrer's formula above. Finally, cross-sectional TEM of the $(Ti_{0.67}Al_{0.33})C_{0.33}$ film showed a similar microstructure, but with smaller grains (100–150 Å) and closer to the surface, the size of the crystallites were further reduced with an almost amorphous feature.

4.5. Formation of MAX phases by solid state reactions

The results from the X-ray analysis of the Ti_3AlC_2 and Ti_3AlC films showed a small contribution from Ti_2AlC (see Sections 4.2 and 4.3). In order to investigate if this phase is

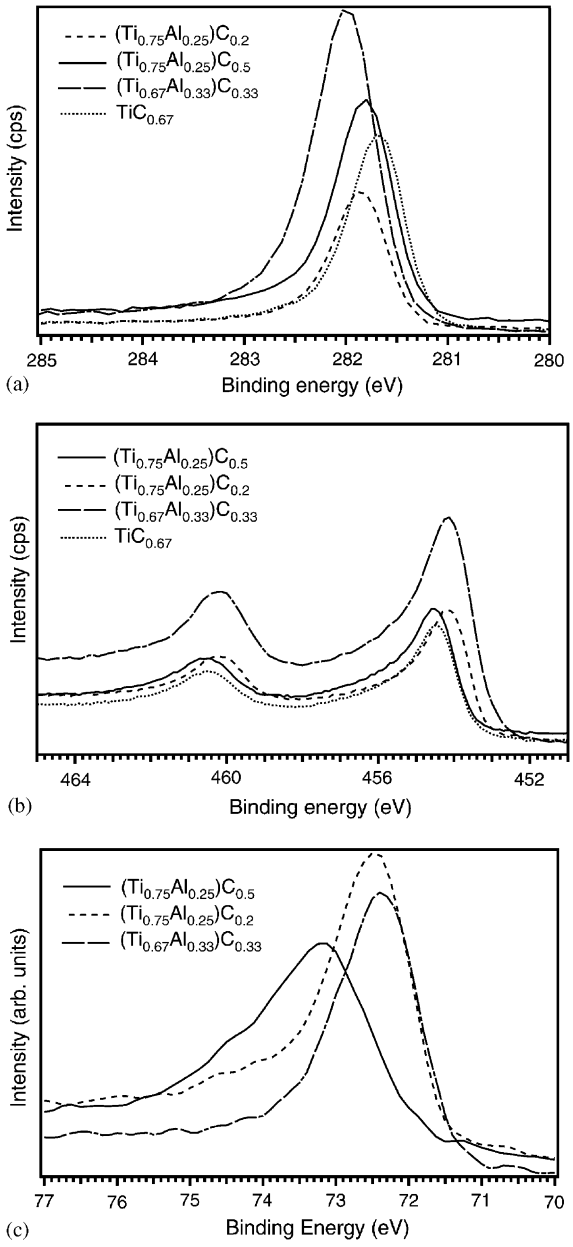

Fig. 11. XPS-measurements of $(Ti_{0.75}Al_{0.25})C_{0.5}$, $(Ti_{0.75}Al_{0.25})C_{0.25}$, $(Ti_{0.75}Al_{0.33})C_{0.33}$ (Ti_2AlC MAX-phase) and TiC: (a) a typical carbide C(1s) peak at ~281 eV. Slightly shifted for the ternary films due to Al–C interactions. (b) Ti(2p) peak positioned at ~454.5 eV. (c) Al(2p) peak shifted towards higher binding energy for the $(Ti_{0.75}Al_{0.25})C_{0.5}$ film due to more pronounced Al–C interactions compared with the $(Ti_{0.75}Al_{0.25})C_{0.25}$, $(Ti_{0.75}Al_{0.33})C_{0.33}$ films.

formed as an interfacial layer between the α-Al_2O_3 substrate and the TiC seed-layer, we deposited a 200 Å thick TiC-layer on an α-Al_2O_3 substrate at 900 °C.

The reaction path between TiC and Al_2O_3 was then investigated by isothermal annealing. A θ–2θ scan of the deposited film shows peaks of $\{\ell\,\ell\,\ell\}$ type from TiC, but also peaks from $Ti_2AlC(0\,0\,2)$, $Ti_2AlC(0\,0\,4)$, and $Ti_2AlC(0\,0\,6)$. This indicates that a solid-state reaction takes place between the TiC seed layer and the α-Al_2O_3 substrate and that the interlayer has grown with a preferred orientation. To investigate whether the composition in the interface layer corresponds to Ti_2AlC, High-Angle Annular Dark-Field (HAADF) microscopy and EDX analysis was performed on a cross-section of a Ti_2AlC film deposited on α-Al_2O_3 with a TiC seed layer at 900 °C. Fig. 13 shows the result of the analysis. The contrast in the HAADF picture arises from the distribution of the elements, where areas with heavier elements appear brighter. The inset in the figure shows the results of the EDX line scan for Al and Ti. In the scan, four areas, labelled 1–4, can be seen. Area 1 corresponds to the substrate followed by area 2 where the interface layer starts. In this area, that is about 100 Å thick, the Ti and Al content reaches a level that is equal to that of the Ti_2AlC film (see area 4). Area 3 corresponds to the TiC seed layer where the Al content is zero. The HAADF micrograph clearly shows that there is an inter-diffusion process of Al and Ti at the substrate. This level of activity at the interface has earlier been observed in studies on the reactivity of Ti metal towards Al_2O_3. Depending on the reaction conditions can, e.g., intermetallics, oxides and solid solutions form [50].

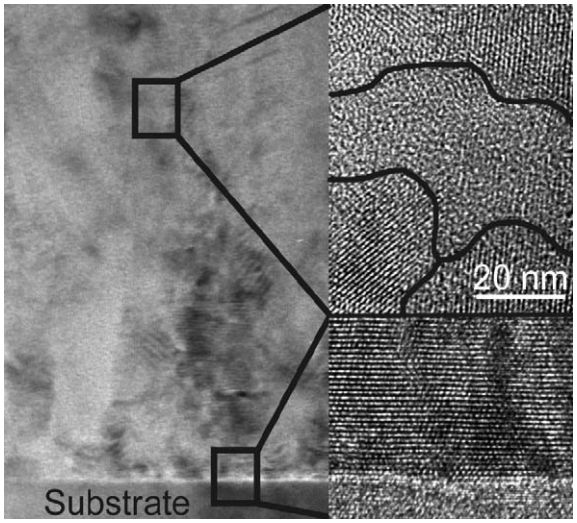

Fig. 12. Cross-sectional TEM images of $(Ti_{0.75}Al_{0.25})C_{0.5}$ film showing (left) overview and (bottom right) a detail from the initial epitaxial growth that turns over to polycrystalline growth (upper right).

5. Conclusions

We have studied the deposition of ternary compounds in the Ti–Al–C system. Epitaxial and almost phase pure films of the MAX phases Ti_3AlC_2 and Ti_2AlC as well as the perovskite carbide Ti_3AlC were deposited on $Al_2O_3(0\,0\,\ell)$ substrates with a $TiC(\ell\,\ell\,\ell)$ seed layer. The formation of the MAX phases was strongly temperature dependent and required temperatures above 800 °C. In contrast, the Ti_3AlC phase could be deposited at lower temperatures

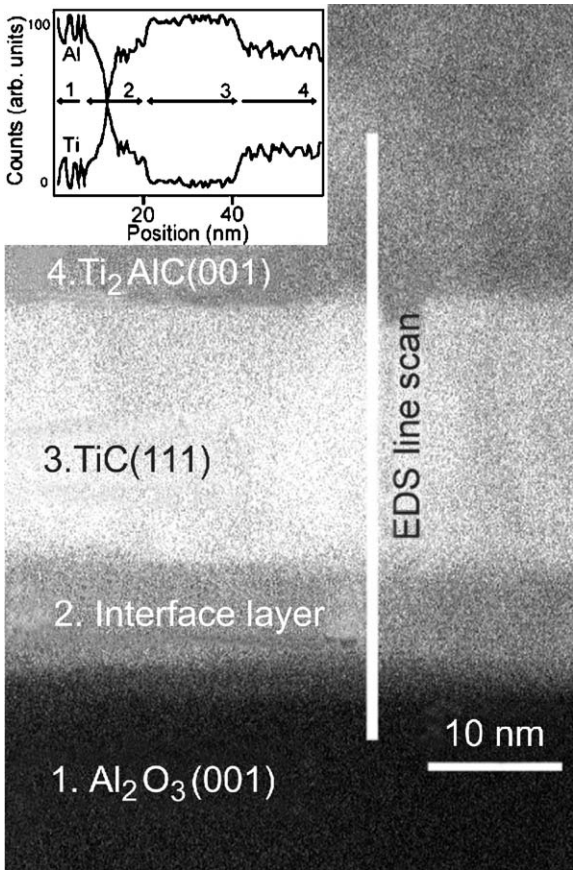

Fig. 13. Solid-state reaction: HAADF-micrograph of Ti_2AlC film (4) deposited on a Al_2O_3 substrate (1) with a seed layer of TiC (3) at 900 °C. The EDX line scan (inset) shows that the interface region (2) has the same composition as in the actual film (4), i.e. a solid-state reaction takes place between the Al_2O_3 substrate and the TiC seed layer.

and epitaxial films of this phase was observed also at 300 °C.

The results indicate that the MAX-phase growth is sensitive to the mobility conditions of the elements participating to form the structure. This includes the observation of random stacking sequences in some layers of the films and the formation of cubic (Ti,Al)C grains during growth. The overall composition of these grains is comparable to the MAX phase, but represent a metastable structure. The reason for forming the simpler cubic phase is due to the kinetic limitations during deposition at relatively low substrate temperatures where the formation of the MAX phase with is large unit cell requires a considerable diffusion rate of atoms during growth. Competitive growth between MAX-phase and cubic (Ti,Al)C was also observed during the nucleation stage. As the Al-target is switched on, the deposition starts with the growth of cubic (Ti,Al)C. The MAX-phases nucleates after a delay period. This type of delayed nucleation has also been observed in the Ti–Si–C system and may be an inherent feature in MAX-phase deposition. It is likely that the A-element (e.g. Al or Si) has to diffuse and segregate to the surface of the growing film and that MAX phase nucleation only can start when a critical surface concentration has been reached.

MAX phases could not be deposited at temperatures below 800 °C. As discussed above, this is probably due to the requirement of high diffusion rates for the formation of the rather complex MAX-phase structures. At lower temperatures a solid solution of Al in TiC is formed. This ternary (Ti,Al)C phase has an Al-content which, considerably higher than the maximum solubility given by the phase diagram. This metastable composition is formed due to low diffusion rates below 800 °C and it is conceivable to assume the film should decompose into the equilibrium phases after a high-temperature annealing. It is interesting to note that the cubic (Ti,Al)C film is a direct parallel to the well-known (Ti,Al)N phases used as wear-resistant coatings by manufacturing industry today. To the knowledge of the authors this is the first report on single-phase (Ti,Al)C films and their physical and chemical properties needs to be further explored. It should be pointed out, however, that there are structural similarities between the perovskite Ti_3AlC and (Ti,Al)C phases. Ti_3AlC can be described as an ordered solid solution of Al in TiC with the total composition $(Ti_{0.75}Al_{0.25})C_{0.25}$ while (Ti,Al)C can be described as a random solid solution of Al on the Ti sites and broad homogeneity range of carbon on the octahedral sites.

Acknowledgments

The Swedish Foundation for Strategic Research (SSF), The Swedish Research Council (VR) and The Swedish Agency for Innovation Systems (VINNOVA) are acknowledged for financial support.

References

[1] N.V. Tzenov, M.W. Barsoum, J. Am. Ceram. Soc. 83 (2000) 825.
[2] W. Jeitschenko, H. Nowotny, Monatsh. Chem. 98 (1967) 329.
[3] V.H. Nowotny, Prog. Solid State Chem. 5 (1971) 27.
[4] M.W. Barsoum, T. El-Raghy, Am. Sci. 89 (2001) 334.
[5] M.W. Barsoum, Prog. Solid State Chem. 28 (2000) 201.
[6] Y. Zhou, Z. Sun, Phys. Rev. B 61 (2000) 12570.
[7] Y. Zhang, G.P. Ding, Y.C. Zhou, B.C. Cai, Mater. Lett. 55 (2002) 285.
[8] Z. Sun, Y. Zhou, M. Li, Acta Mater 49 (2001) 4347.
[9] S. Myhra, J.W.B. Summers, E.H. Kisi, Mater. Lett. 39 (1999) 6.
[10] Y. Zhou, Z. Sun, X. Wang, S. Chen, J. Phys.: Condens. Matter 13 (2001) 10001.
[11] Z. Sun, D. Music, R. Ahuja, S. Li, J.M. Schneider, Phys. Rev. B 70 (2004) 092102.
[12] T. El-Raghy, P. Blau, M.W. Barsoum, Wear 238 (2000) 125.
[13] P. Eklund, J. Emmerlich, H. Högberg, O. Wilhelmsson, P. Isberg, J. Birch, P. O. Å. Persson, U. Jansson, L. Hultman, unpublished.
[14] P. Villars, A. Prince, H. Okomoto, Handbook of Ternary Alloy Phase Diagrams, vol. 4, ASM International, London, 1995.
[15] M.A. Pietzka, J.C. Schuster, J. Phase Equ. 15 (1994) 392.
[16] S. Riaz, H.M. Flower, D.R.F. West, Mater. Sci. Technol. 16 (2000) 984.
[17] F.M. Samir, Y.L. Petitcorps, J. Etourneau, J. Mater. Chem. 7 (1997) 99.

[18] W.H. Tian, M. Nemoto, Intermet 5 (1996) 237.
[19] T. He, Q. Huang, A.P. Ramirez, Y. Wang, K.A. Regan, N. Rogado, M.A. Hayward, M.K. Haas, J.S. Slusky, K. Inumara, H.W. Zandbergen, N.P. Ong, R.J. Cava, Nature 411 (2001) 54.
[20] D.P. Young, M. Moldovan, P.W. Adams, Phys. Rev. B 70 (2004) 064508.
[21] M. Witthaut, R. Cremer, A.v. Richthofen, D. Neuschutz, J. Anal. Chem. 361 (1998) 639.
[22] W.-D. Munz, J. Vac. Sci. Technol. A 4 (1986) 2717.
[23] A. Hörling, L. Hultman, M. Odén, J. Sjölén, L. Karlsson, Surf. Coat. Technol. 191 (2005) 384.
[24] O. Wilhelmsson, J.-P. Palmquist, T. Nyberg, U. Jansson, Appl. Phys. Lett. 85 (2004) 1066.
[25] W.C. Oliver, G.M. Pharr, J. Mater. Res. 7 (1992) 1564.
[26] Z. Sun, R. Ahuja, S. Li, J.M. Schneider, Appl. Phys. Lett. 83 (2003) 899.
[27] J.-P. Palmquist, S. Li, P.O.Å. Persson, J. Emmerlich, O. Wilhelmsson, H. Högberg, M.I. Katsnelson, B. Johansson, R. Ahuja, O. Eriksson, L. Hultman, U. Jansson, Phys. Rev. B 70 (2004) 165401.
[28] Y.C. Zhou, H.Y. Dong, X.H. Wang, S.Q. Chen, J. Phys.: Condens. Matter 12 (2000) 9617.
[29] J.Y. Wang, Y.C. Zhou, J. Phys.: Condens. Matter 15 (2003) 5959.
[30] P.E. Blöchl, Phys. Rev. B 50 (1994) 17953.
[31] F.D. Murnaghan, Proc. Natl. Acad. Sci. 30 (1944) 244.
[32] M. Magnusson, J.-P. Palmquist, M. Mattesini, S. Li, R. Ahuja, O. Eriksson, J. Emmerlich, O. Wilhelmsson, P. Eklund, H. Högberg, L. Hultman, U. Jansson, Submitted to Phys. Rev. B.
[33] H. Högberg, P. Eklund, J. Emmerlich, J. Birch, L. Hultman, J. Mater. Res. 20 (2005) 779.
[34] J. Emmerlich, J.-P. Palmquist, H. Högberg, J. Molina, Z. Czigány, S. Sasvári, P.O. Persson, U. Jansson, L. Hultman, J. Appl. Phys. 96 (2004) 4817.
[35] Z.J. Lin, M.J. Zhuo, Y.C. Zhou, M.S. Li, J.Y. Wang, Acta Mater 54 (2006) 1009.
[36] V. Nikolay, M.W. Barsoum, J. Am. Cerm. Soc. 83 (2000) 825.
[37] T. Goto, T. Hirai, Mater. Res. Bull. 22 (1987) 1195.
[38] X.H. Wang, Y.C. Zhou, Acta Mater 50 (2002) 3141.
[39] K. Sangwal, B. Surowska, P. Blaziak, Mater. Chem. Phys. 77 (2002) 511.
[40] B.J. Kooi, R.J. Poppen, N.J.M. Carvalho, J.T.M.D. Hosson, M.W. Barsoum, Acta Mater 51 (2003) 2859.
[41] J.J. Nickl, K.K. Schweitzer, P. Luxenberg, J. Less-Common Met. 26 (1972) 283.
[42] J.M. Molina-Aldareguia, J. Emmerlich, J.-P. Palmquist, U. Jansson, L. Hultman, Scripta Mater 49 (2003) 155.
[43] S. Li, J. Xie, J. Zhao, L. Zhang, Mater. Lett. 57 (2002) 119.
[44] L.E. Toth, Transition Metal Carbides and Nitrides, Academic Press, New York and London, 1971.
[45] Z. Dridi, B. Bouhafs, P. Ruterana, H. Aourag, J. Phys.: Condens. Matter 14 (2002) 10237.
[46] M. Guemmaz, G. Moraitis, A. Mosser, M.A. Khan, J.C. Parlebas, J. Electron. Spectrosc. Relat. Phenom. 83 (1997) 173.
[47] L. Ramqvist, J. Ann. 517 (1968).
[48] R. Hauert, J. Patscheider, M. Tobler, R. Zehringer, Surf. Sci. 292 (1993) 121.
[49] P.W. Shum, Z.F. Zhou, K.Y. Li, Y.G. Shen, Mater. Sci. Eng. B 100 (2003) 204.
[50] A.M. Kliauga, M. Ferrante, J. Mater. Sci. 35 (2000) 4243.